Journal of Alloys and Compounds 803 (2019) 135–144

Contents lists available at ScienceDirect

Journal of Alloys and Compounds

journal homepage: http://www.elsevier.com/locate/jalcom

Acetone-sensing properties of doped ZnO nanoparticles for breath-analyzer applications

Ran Yoo, Yunji Park, Hwaebong Jung, Hyun Jun Rim, Sungmee Cho, Hyun-Sook Lee**, Wooyoung Lee*

Department of Materials Science and Engineering, Yonsei University, 50 Yonsei-ro, Seodaemun-gu, Seoul, 03722, Republic of Korea

ARTICLE INFO

Article history:
Received 3 April 2019
Received in revised form
7 June 2019
Accepted 20 June 2019
Available online 21 June 2019

Keywords:
Al-doped ZnO nanoparticles
Acetone
Deep donor level defects
Breath acetone analyzer

ABSTRACT

We report the effects of various dopants (Al, Co, and Cu) on the acetone-sensing properties of ZnO nanoparticles (NPs) for breath-analyzer applications. Among the different sensing materials, the Al-doped ZnO NPs exhibited the highest sensitivity toward 1 ppm acetone, with a maximum response of 11.8 at 500 °C. This improved sensing performance was related to deep donor-level defects caused by double oxygen vacancies in the Al-doped ZnO NPs, as confirmed by photoluminescence spectra. Thus, Al was a more effective dopant than Cu and Co for enhancing the sensing properties of ZnO NPs for the detection of acetone. We achieved selective detection of 0.5 ppm acetone in air using the Al-doped ZnO NPs incorporated into a miniaturized gas chromatograph (GC). The results indicate that the miniaturized GC integrated with the Al-doped ZnO NPs can be utilized for an acetone breath analyzer.

1. Introduction

Several reports [1–6] have recently discussed the development of new diagnostic methods to identify personal health conditions. For instance, exhaled breath is a source of potential biomarkers for certain diseases. Diabetes is the chronic condition with the most rapidly increasing number of cases, and its presence can be assessed according to the acetone concentration in exhaled breath [2,3]. Typical breath acetone concentrations of healthy humans range from 0.3 to 4 ppm [4,5] but can increase to 1,250 ppm in adults with diabetic ketoacidosis [6]. Currently, the most common method for monitoring diabetes is invasive blood glucose testing to measure blood sugar levels. More advanced diagnostic technologies such as gas chromatography and mass spectrometry have been developed for the detection of exhaled acetone [7–9]. Portable gaseous acetone sensors can promote non-invasive, convenient, cost-effective, and efficient diabetic monitoring.

Metal-oxide semiconductor (MOS) materials are used extensively in gas sensors because of their abundance, high chemical stability, and favorable sensing properties. In recent studies, MOS sensors based on WO_3 [10], SnO_3 [11,12], Co_3O_4 [13], ZnO [14,15], and ZnO/$ZnFe_2O_4$ [16,17] have been explored for detecting acetone in exhaled volatile organic compounds (VOCs). Among the various sensing materials, ZnO is particularly promising and has been studied in one-to three-dimensional structures to enhance its sensing capabilities [18,19]. Furthermore, ZnO has also been used for a wide range of applications such as transistors, memory devices, photodetectors, solar cells, and light-emitting diodes owing to their excellent electronic and optoelectronic properties [20–27]. In ZnO-based chemiresistive sensors, the hierarchical structures of ZnO not only provide large surface-to-volume ratios, but also afford improved gas diffusion and mass transport properties in the sensors. The sensing properties of ZnO can be modulated by changing the particle morphology, the crystal structure, the energy band structure, and the number of surface sites available for gas interaction [28,29]. Doping ZnO with aliovalent metal oxides is an effective technique for altering its electronic structure.

We recently demonstrated Al-doped ZnO nanoparticles (NPs) that exhibited high sensitivity toward the representative VOC acetaldehyde [29] and simulants of chemical warfare agents such as dimethyl methylphosphonate (DMMP) [30] and 2-chloroethyl ethyl sulfide (2-CEES) [31]. In particular, 1 at% Al-doped ZnO NPs exhibited extremely high sensing responses to acetaldehyde ($R = 2,250$), DMMP ($R = 4,341$), and 2-CEES ($R = 996$) at 10 ppm and low sensing responses to NH_3, CO, toluene, benzene, NO, and NO_2.

* Corresponding author.
** Corresponding author.
E-mail addresses: h-slee@yonsei.ac.kr (H.-S. Lee), wooyoung@yonsei.ac.kr (W. Lee).

https://doi.org/10.1016/j.jallcom.2019.06.254
0925-8388/

Here, the sensing response (R) is defined as $\Delta R/R_g$ ($\Delta R = R_a - R_g$), where R_a and R_g are the resistances of the sensor in air and in an environment containing target gas, respectively. That is, the Al-doped ZnO NPs were more sensitive to specific gases such as acetaldehyde [29], DMMP [30], and 2-CEES [31], which have high dipole moments as molecular gases, than to NH_3, CO, toluene, benzene, NO, and NO_2. Our results indicate that the Al-doped ZnO NPs are more responsive to specific gases with high molecular dipole moments [32]. This is attributed to the strong dipole–dipole interaction between the gas dipole and negatively charged oxygen vacancies on the surfaces of ZnO NPs [33].

As MOS sensors suffer from a lack of selectivity for various gases, the Al-doped ZnO NPs do not show selectivity for acetaldehyde [29], DMMP [30], or 2-CEES [31]. To circumvent the selectivity problem of the ZnO NP-based sensor, we recently developed a miniaturized gas chromatograph (GC) integrated with Al-doped ZnO quantum dots (QDs) [34] for the selective sensing of various gases. We found that acetone [34], 2-CEES [35], acetylene, and isoprene [36] could be separated effectively in the miniaturized GC using ZnO-based QDs. Our extensive study of doped ZnO NPs for the detection of acetone is necessary for their application in an acetone breath analyzer.

In this work, we investigated the doping effects of Al, Co, and Cu on the acetone-sensing properties of ZnO NPs synthesized via a hydrothermal method for the detection of low concentrations (0.01–10 ppm) of acetone under both dry and humid conditions. Al-doped ZnO NPs were found to have the highest sensing response to acetone. We discussed the enhanced sensing mechanism of the Al-doped ZnO NPs with regard to the transitions of defect states. We tested the sensitive detection of acetone using the miniaturized GC integrated with the Al-doped ZnO NPs for breath-analyzer applications.

2. Experiment

2.1. Synthesis and characterization of sensing materials

Undoped ZnO NP powder and Al-, Cu-, and Co-doped ZnO NP powders were synthesized via a hydrothermal method. To synthesize the Al-, Cu-, and Co-doped ZnO NPs, either aluminum acetate ($Al(C_2H_3O_2)_3$, Sigma–Aldrich), copper acetate monohydrate ($Cu(CO_2CH_3)_2$, Sigma–Aldrich), or cobalt acetate tetrahydrate ($(CH_3COO)_2Co\cdot 4H_2O$, Sigma–Aldrich) was added to the zinc acetate solution with stirring at a 1% atomic ratio of the dopant to Zn. This particular doping concentration was chosen because it exhibited the best sensing property among the various doping concentrations (0.5–2.0 at%) of Al-doped ZnO NPs [31]. After the hydrothermal reaction, the synthetic powder was centrifuged and cleaned with methanol. It was then dried at 90 °C for 60 min and annealed at 350 °C for 30 min in a H_2 atmosphere. The synthesis procedure was previously described in detail [29–31].

Characterizations of the as-synthesized NPs, such as their particle size and microstructure, were performed using transmission electron microscopy (TEM; JEM ARM200F, JEOL). The crystal structures of the powders were examined via X-ray diffraction (XRD; Ultima IV/ME 200DX, Rigaku) with Cu Kα radiation. The optical properties of the samples were analyzed via photoluminescence (PL) measurements. The PL spectra were obtained using a spectrometer (Horiba) after the samples were excited by a He–Cd laser ($\lambda = 325$ nm).

2.2. Gas sensing test

For the gas-sensing measurements in a tube furnace system, the sensor devices (8.5 mm × 8.5 mm) were fabricated as follows. A mixture of the annealed product and α-terpineol paste was dispersed onto interdigitated Pt electrodes through a dropping method on a SiO_2 substrate. Fig. 1(a) and (b) show the schematic of

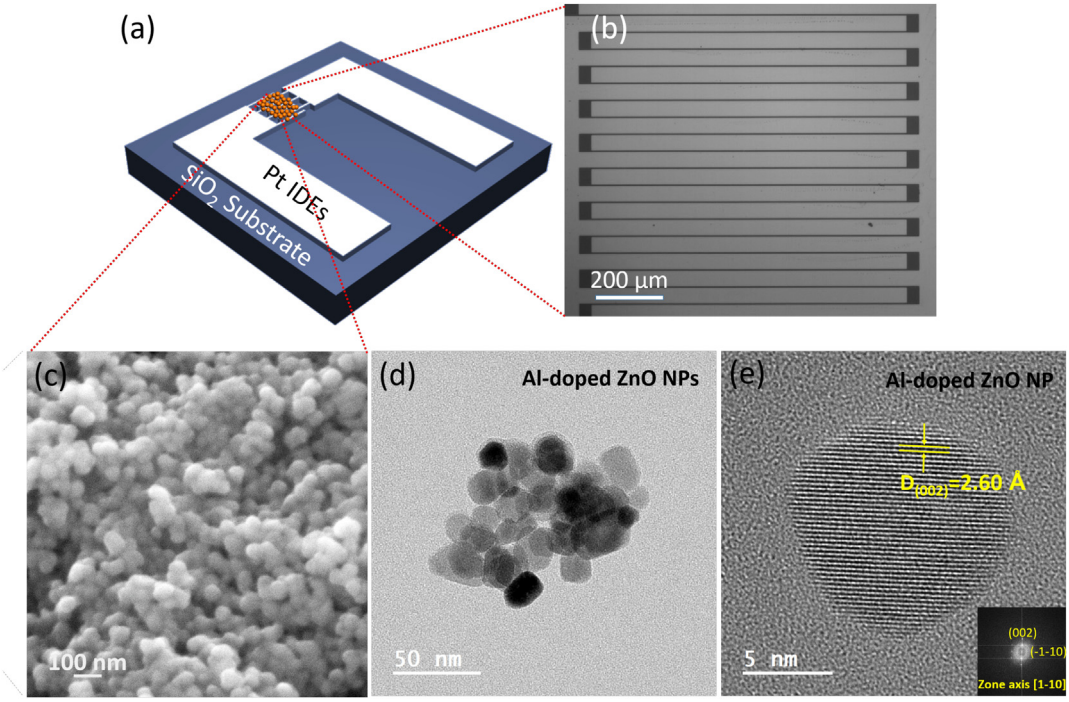

Fig. 1. (a) Schematic of the sensor device; (b) SEM image of the actual Pt electrodes patterned on the SiO_2 substrate; (c) SEM image of the Al-doped ZnO NPs spread on the electrode surface after annealing; (d) TEM image of Al-doped ZnO NPs; (e) high-resolution TEM image of an isolated Al-doped ZnO NP. The inset shows the FFT pattern of a single Al-doped ZnO NP.

the sensor device and the SEM image of the actual Pt electrodes patterned on the SiO_2 substrate, respectively. Subsequently, a two-step heat treatment of 300 °C for 1 h and 600 °C for 1 h was performed to remove the α-terpineol paste and enhance the stability of the sensor. Fig. 1(c) shows the SEM image of the Al-doped ZnO NPs spread on the electrode surface after the annealing. The gas-sensing properties were measured using a gas-detecting furnace system consisting of a tube furnace (Korea Vacuum Tech.,Korea), mass flow controllers, a current source (Keithley 6220), and a nanovolt-meter (Keithley 2182), as described in previous works [29–31]. The resistance signals were obtained from two Pt probes connected to the current source and voltmeter with a constant current supply of 10 nA for a time interval of 1 s. The acetone gas concentration in synthetic air was maintained between 0.1 and 10 ppm by controlling the partial pressure using mass flow controllers. The gas flow rate was maintained at 1000 sccm. All the gas-sensing measurements were conducted at operating temperatures of 300–550 °C. The sensing response is defined as $\Delta R/R_g$ ($\Delta R = R_a - R_g$), where R_a and R_g are the resistances of the sensor in air and in the gaseous mixture of pure air and the target gas, respectively.

For the gas-sensing measurements in a miniaturized GC system, the nanoparticle powder mixed with α-terpineol paste was loaded onto the interdigitated Pt electrodes patterned on an Al_2O_3 substrate (0.5 mm × 0.25 mm). After loading, the sensor was heated at 300 °C for 30 min and 600 °C for 30 min. The gas-sensing measurements were performed using a miniaturized GC integrated with the ZnO-based NP sensor as described in previous works [34,35]. A packed column was used as a GC column inside the device. The column was packed with a filler (CarboBlack B) coated with a stationary phase (CarboWax 20 M). The inner diameter and length of the column were adjusted to 0.15 cm and 20 cm, respectively, to shorten the retention time of the target gas. The operating temperature of the column was kept at room temperature (30 °C). Acetone was injected directly into the miniaturized GC device without pre-concentration. Dry air was used as a carrier gas at a flow rate of 20 sccm. The sampling volume of dry air and acetone was limited to 1 ml. The sensing characteristic was evaluated as a sensor signal (log(R)) by converting the logarithm of the sensor resistance.

3. Results and discussion

The morphology and microstructure of the prepared Al-doped ZnO NPs were analyzed using TEM, and the results are shown in Fig. 1. The TEM image shown in Fig. 1(d) reveals that the NPs were not exactly spherical in shape, and the particle sizes were in the range of 15–30 nm. A high-resolution TEM image of an isolated Al-doped ZnO NP is shown in Fig. 1(e). According to this image, the interplanar spacing was estimated to be 2.60 Å, which corresponds to the (002) lattice plane of ZnO. The fast Fourier transform (FFT) pattern along the [1–10] zone axis shown in the inset of Fig. 1(e) confirms that the NP had a single-crystalline hexagonal ZnO structure.

The phase structures of the undoped ZnO NPs and Al-, Cu-, and Co-doped ZnO NPs were characterized via XRD and are compared in Fig. 2. The XRD patterns show that all the ZnO NPs had hexagonal wurtzite structures (JCPDS: #36-1451), with three of the strong diffraction peaks corresponding to the (100), (002), and (101) lattice planes. No other secondary phases or impurity peaks are observed, indicating that the dopant was well-integrated into the lattice sites. To examine the effect of the dopant ions in the pristine ZnO lattice, the strongest peak of the (101) plane of the wurtzite structure is studied (inset of Fig. 2). It appears that for all of the doped ZnO NPs studied in this work, the (101) peak position was slightly shifted to a higher 2θ degree relative to that of pure ZnO

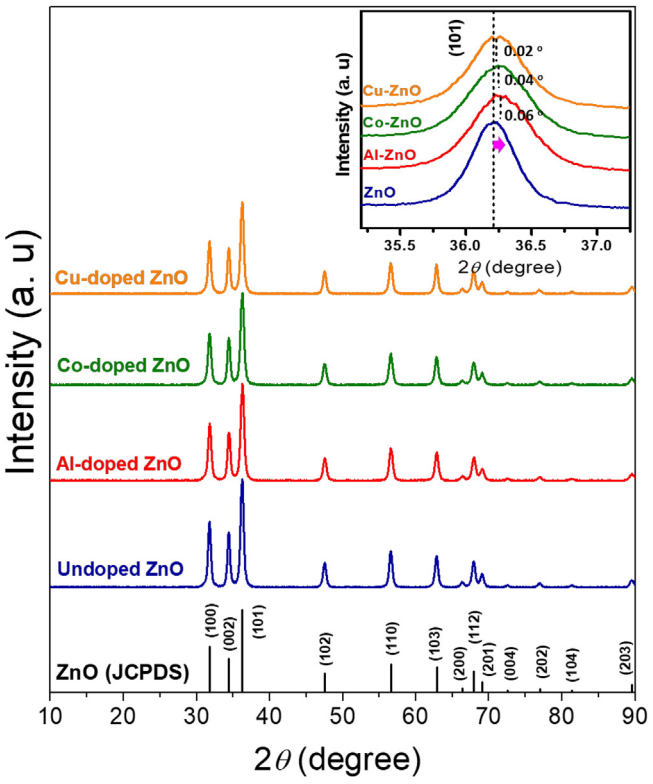

Fig. 2. XRD patterns of undoped (blue), Al-doped (red), Co-doped (green), and Cu-doped (orange) ZnO NPs. The inset shows a magnified image of the (101) peaks, which are slightly shifted to larger angles for the doped samples. (For interpretation of the references to colour in this figure legend, the reader is referred to the Web version of this article.)

NPs. This shift was ~0.06°, ~0.04°, and ~0.02° for the Al-, Co-, and Cu-doped ZnO NPs, respectively. The shift to higher angles is attributed to the smaller atomic radii of the Al^{3+} (0.53 Å), Co^{2+} (0.65 Å), and Cu^{2+} (0.73 Å) ions compared with that of Zn^{2+} (0.74 Å), which reduced the interlayer spacing of ZnO along the (101) axis. However, the shift of the (101) peak position for the Cu-doped ZnO NPs was smaller because the ionic radius of Cu^{2+} (0.73 Å) is similar to that of Zn^{2+}. The shifting of the diffraction peak indicates the incorporation of Al, Co, and Cu into the ZnO lattice.

The sensing properties of the ZnO NPs fabricated with and without the dopants upon exposure to 1 ppm acetone were analyzed at different temperatures (Fig. 3). Fig. 3(a) shows the maximum sensing responses of all the tested ZnO NPs with respect to the operating temperature. The sensing responses of all the ZnO NPs synthesized with and without dopants increased as the operating temperature increased to 500 °C but decreased significantly at 550 °C. Thus, the highest responses of all the samples were achieved at 500 °C, which is the optimum operating temperature of the sensor for 1 ppm acetone. As the operating temperature increases, the high molecular activity and rapid conversion of the adsorbed oxygen species (e.g., O_2 (gas) to $2O^-$ (ads)) on the surface of the ZnO NPs contributed to the enhancement of surface chemical reactions, yielding improved responses [16]. However, a high temperature exceeding the optimum operating temperature inhibited gas adsorption, reducing the response, as shown in Fig. 3(a). Fig. 3(b)–3(f) show the variations in the sensing responses of the undoped and Al-, Co-, and Cu-doped ZnO NPs upon exposure to 1 ppm acetone at different operating temperatures of 300, 350, 400, and 500 °C. Among the samples, the Al-doped ZnO NPs exhibited the highest sensing response to 1 ppm acetone at all the

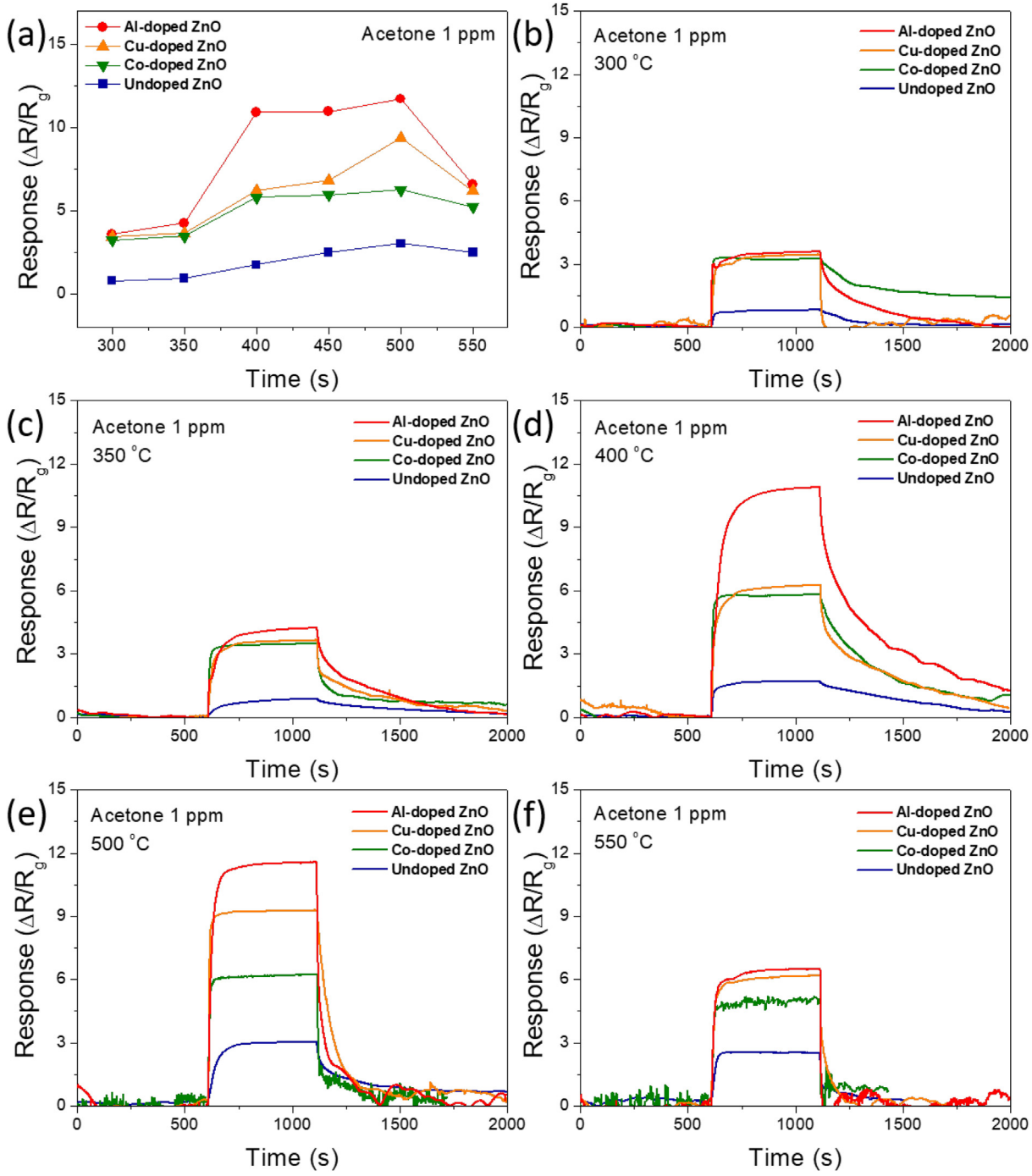

Fig. 3. (a) Maximum sensing response of the undoped and Al-, Co-, and Cu-doped ZnO NPs toward 1 ppm acetone with respect to the operating temperature in the range of 300–550 °C; (b)–(f) variation in the sensing responses of all ZnO NPs upon exposure to 1 ppm of acetone at 300, 350, 400, 500, and 550 °C.

temperatures, as can be observed from Fig. 3(a). The Al-doped ZnO NPs showed the strongest response of 11.8 to 1-ppm acetone at the optimal temperature of 500 °C, as shown in Fig. 3(a).

The sensing properties of the samples were analyzed with the variation of the acetone concentration at the optimum working temperature of 500 °C (Fig. 4). Fig. 4(a) shows the sensing responses of the undoped and doped ZnO NPs at various acetone concentrations in the range of 0.01–10 ppm at 500 °C. The sensing responses of all the ZnO NPs increased linearly with the increase of the acetone concentration. The sensitivities of the samples were estimated by a linear fitting in the range of 0.5–10 ppm. The estimated sensitivities were approximately 4.9, 3.3, 1.9, and 1.3 for the Al-doped, Cu-doped, Co-doped, and undoped ZnO NPs, respectively. For all the cases, the linear correlation coefficient R^2 was close to 1. The results indicate that the Al-doped ZnO NPs had the highest sensitivity. Fig. 4(b)–4(e) show the sensing responses of the undoped ZnO and Co-, Cu-, and Al-doped ZnO NPs as a function of the acetone concentration (0.01–10 ppm) at the optimal operating temperature of 500 °C. For all the NPs, the sensing response transience decreased with a decrease in the acetone concentration from 10 to 0.01 ppm at 500 °C (Fig. 4(a)). At 10 and 0.01 ppm, the Al-doped ZnO NPs exhibited responses of ~55 and ~3, respectively.

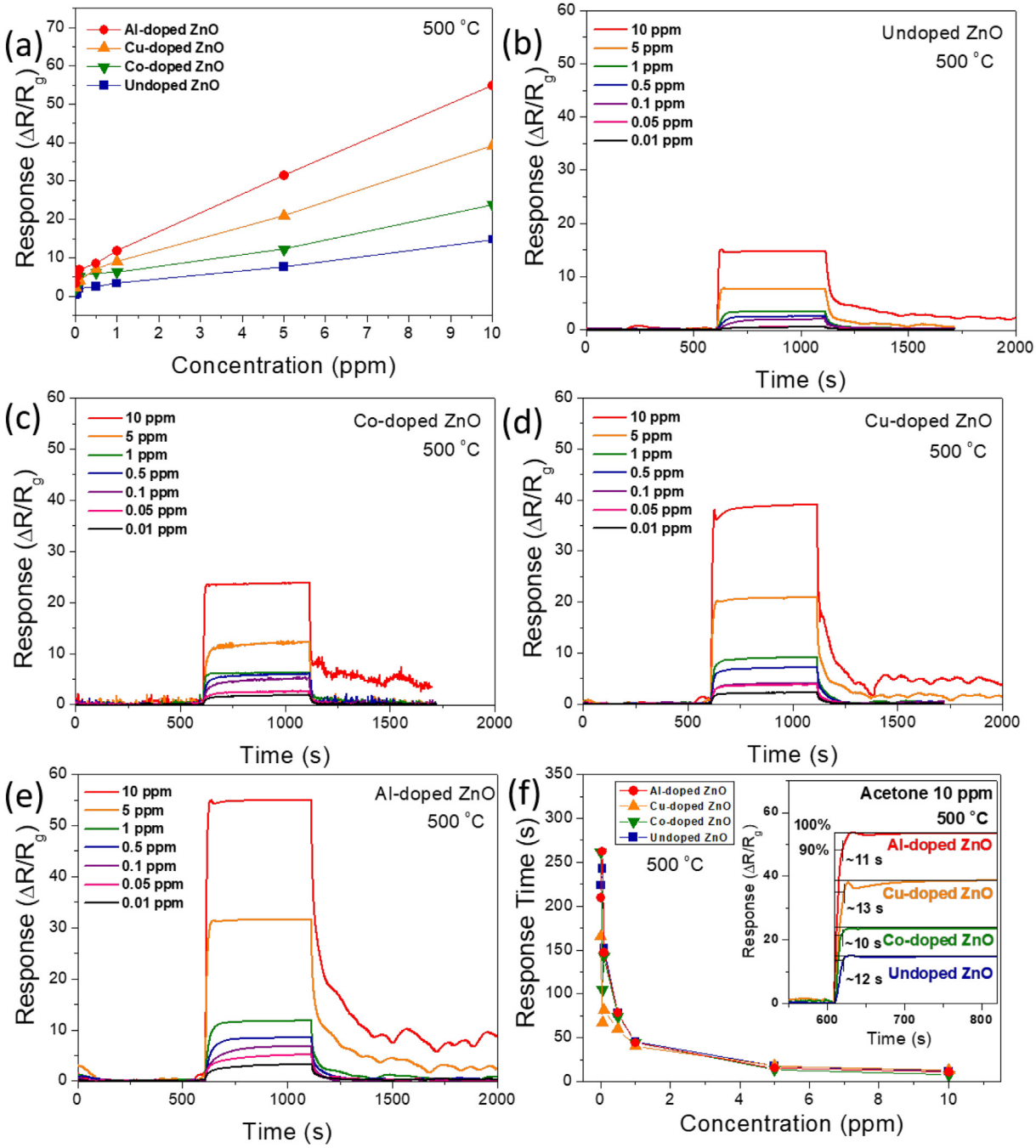

Fig. 4. (a) Sensing responses of the undoped and Co-, Cu-, and Al-doped ZnO NPs to different concentrations of acetone in the range of 0.01–10 ppm at the optimal operating temperature of 500 °C; (b)–(e) variations in the responses of the undoped and Co-, Cu- and Al-doped ZnO NPs during the detection of acetone at different acetone concentrations in the range of 0.01–10 ppm at 500 °C; (f) response time as a function of the acetone concentration (0.01–10 ppm) at 500 °C. The inset shows the estimation of the response time of all the samples upon exposure to 10 ppm acetone.

This means that the Al-doped ZnO NPs sufficiently detected a low concentration (0.01 ppm) of acetone.

The response times of the undoped and doped ZnO NPs exposed to various acetone concentrations were estimated as the time required for the resistance change to reach 90% of the total resistance change. It was obtained from the response vs. time curves of the NPs (Fig. 4(b)–4(e)). The inset of Fig. 4(f) indicates the response time of the undoped and doped ZnO samples upon exposure to 10 ppm acetone at 500 °C. At 10 ppm acetone, the response times for all the samples were found to be within the range of 10–13 s. Fig. 4(f) shows the response time of the samples at various acetone concentrations (0.01–10 ppm) at 500 °C. The response time increased with an increase in the acetone concentration. The Al-doped ZnO NPs showed the response times of approximately 262, 147, 78, 44, 15, and 11 s at the acetone concentrations of 0.05, 0.1, 0.5, 1, 5, and 10 ppm, respectively.

The recovery time of the samples was estimated as the time required to return to 90% of the original resistance after the release of the test gas. Unlike the response time, the recovery time of the samples increased with an increase in the acetone concentration

(Fig. 4(b)–4(e)). The Al-doped ZnO NPs showed the recovery times of approximately 70, 113, 181, 493, and 597 s at the acetone concentrations of 0.1, 0.5, 1, 5, and 10 ppm, respectively. This is attributed to the acetone gas molecules remaining on the detecting surface of the ZnO NPs after the chemical adsorption of the gas molecules. Therefore, further study is required to identify the reason for the long resting time required for the desorption of all these molecules from the detecting surface.

According to the sensing results of the prepared ZnO NPs (Figs. 3 and 4), the doped ZnO NPs had a higher sensing response than the undoped ZnO NPs, and the Al-doped ZnO NPs exhibited the highest response among the doped ZnO NPs. Compared with the undoped ZnO NPs, the enhancement of the sensing response for the Al-doped ZnO NPs was explained by the increase in the conductivity and oxygen vacancies of the ZnO NPs due to Al dopant substitution [30,31]. The superiority of the Al-doped ZnO NPs is attributed to the large number of valence electrons in Al^{3+} compared to the other doping (Co^{2+} and Cu^{2+}) elements.

To further investigate the transitions of the defect states in the ZnO NPs fabricated with various dopants, the PL spectra of undoped and Al-, Cu-, and Co-doped ZnO NPs were obtained at a constant laser power with an excitation wavelength of 325 nm at room temperature. In Fig. 5(a), all the measured spectra exhibit similar features, with three emission bands between 350 and 450 nm,

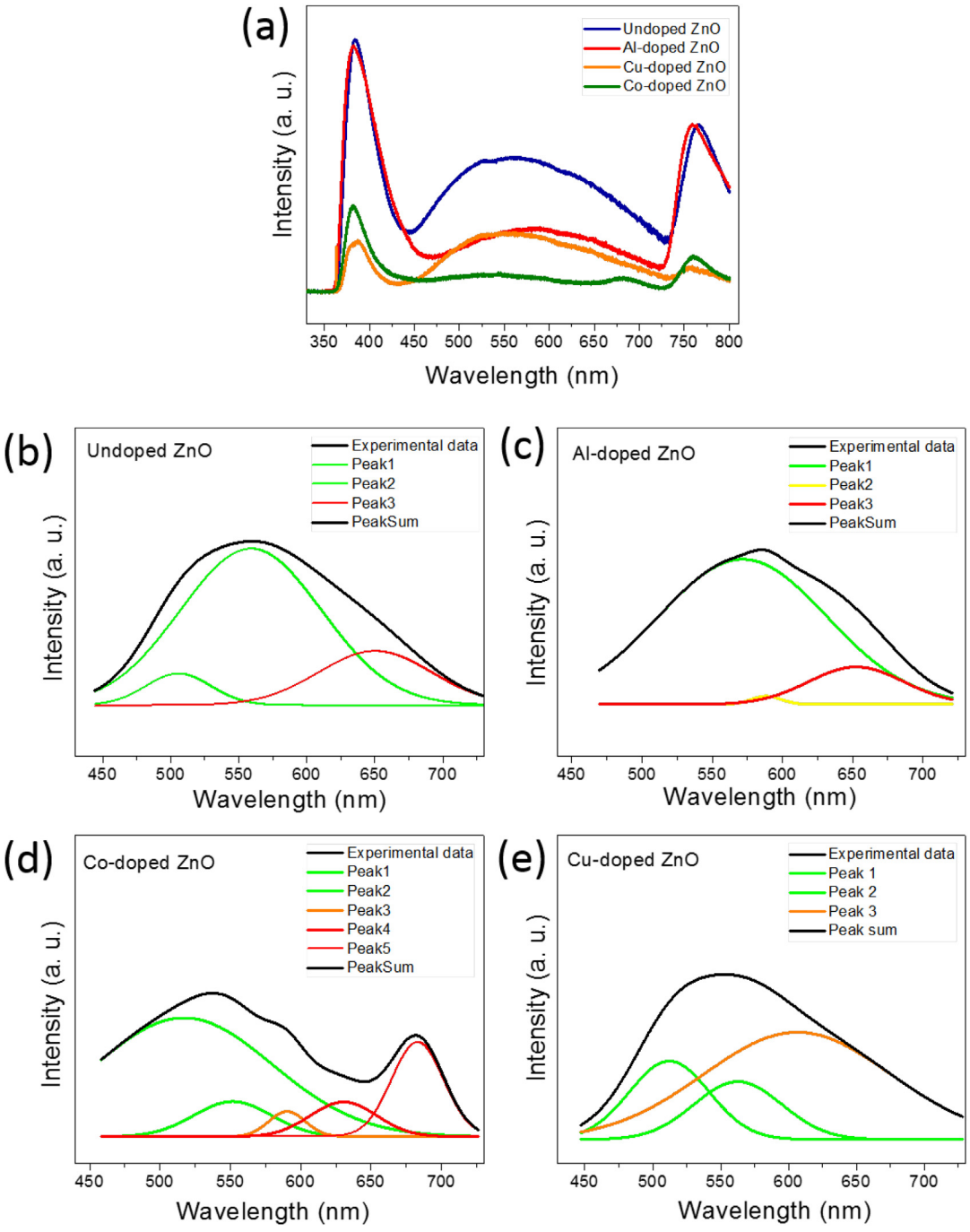

Fig. 5. (a) PL spectra of undoped (blue), Al-doped (red), Cu-doped (orange), and Co-doped (green) ZnO NPs obtained using an excitation wavelength of 325 nm; (b)–(e) Gaussian deconvolutions of the PL spectra for all samples. (For interpretation of the references to colour in this figure legend, the reader is referred to the Web version of this article.)

between 450 and 750 nm, and between 750 and 800 nm. The ultraviolet emission band at 350–450 nm was related to the near-band-edge emission arising from free exciton recombination [37] and did not shift for any of the samples. The middle band at 450–750 nm indicates deep-level emission, which is attributed to the intrinsic and extrinsic defects from the recombination of electrons in the conduction band and holes in the valence band [38].

The broad bands in the range of 450–750 nm in the PL spectra were deconvoluted via Gaussian fitting, as shown in Fig. 5(b)–(e). In a PL spectrum, green, yellow, orange, and red emissions occur in the wavelength ranges of 498–569 nm, 570–589 nm, 590–619 nm, and 620–750 nm, respectively [39]. The emissions of the pure ZnO NPs are centered at 505, 559, and 650 nm, corresponding to two green peaks and one red peak (Fig. 5(b)). The emission spectra of ZnO NPs with Al and Cu dopants show green, yellow, and red peaks and green and orange peaks, respectively. Interestingly, the Co-doped ZnO NPs exhibit a broadband PL spectrum with five emission peaks. According to a previous report [39], a deep donor-level defect occurs in the presence of a singly charged oxygen vacancy (V_O^+) for green light, a doubly charged oxygen vacancy (V_O^{++}) for yellow light, and adsorbed oxygen for orange and red light [39]. Among these, oxygen vacancies significantly affect the sensing properties of ZnO [30,31]. The yellow emission observed only in the case of the Al-doped ZnO NPs supports the proposed mechanism for the improvement in the sensing response, indicating that a large number of V_O^{++} donors facilitated the adsorption of oxygen ion species on the surface and that a large number of atoms participated in the surface chemical reactions [40]. Consequently, the Al dopants caused electronic transitions in the defect states, particularly to form doubly charged oxygen vacancies, which affected the sensing performance of the ZnO NPs. Furthermore, the Al^{3+} dopant atoms in the lattice of the ZnO NPs acted as donors of conducting electrons, causing the NPs to adsorb more oxygen ion species (i.e. reactive sites for gas molecules) on their surfaces compared to Cu and Co. This suggests that Al is a more effective dopant than Cu and Co for enhancing the acetone sensing properties of ZnO NPs.

The schematics in Fig. 6 illustrate the sensing mechanism for acetone detection based on the aforementioned results. In principle, the resistance of the sensor changes during the adsorption and desorption of gas molecules on the surface of the Al-doped ZnO material, as shown in Fig. 6(a). Under exposure to air, oxygen molecules are adsorbed on the surface of the Al-doped ZnO NPs in the sensor; they accept electrons from the NP conduction bands to form an absorbed surface oxygen ion species. This induces the formation of a thick depletion layer with an increasing potential barrier, which increases the resistance of the sensor. However, when the Al-doped ZnO NPs are exposed to acetone (CH_3COCH_3), a charge exchange occurs between the acetone and the absorbed surface oxygen ion species (O^{2-}). Consequently, the barrier height for electrons in the conduction band is changed, depending on the doping material and the quantity of adsorbed oxygen [15]. The reactions are described as follows:

$$CH_3COCH_{3\ (gas)} \xrightarrow{ZnO} C_{3x}H_{6x}O_xZnO \quad (1)$$

$$CH_3COCH_3(ads) + 8O^-\ (ads) \leftrightarrow 3CO_2(gas) + 3H_2O(gas) + 8e^- \quad (2)$$

When acetone is oxidized, the electrons are released into the conduction band, simultaneously forming CO_2 and H_2O, and the resistance of the Al-doped ZnO NPs decreases. The thickness of the depletion layer and the resistance of the sensor also decrease, as shown in Fig. 6(b) [19]. Consequently, the addition of higher valence Al dopants to ZnO promotes the formation of doubly charged oxygen vacancies in ZnO and a large number of oxygen ion species on the surface of ZnO. This leads to the generation of a large number of active adsorption centers for detecting the test gas molecules and the enhancement of the surface reactions by reducing the activation energy [41,42], which significantly improves the sensor response of the Al-doped ZnO NPs compared to others, such as pure and Cu- and Co-doped ZnO NPs.

In human breath, some analytes (e.g., NH_3, CO, or isoprene) are present at high ppb or even ppm levels [43] and high relative humidity (RH) levels (~89%–97%) [44]. Fig. 7 presents the sensing performance of the Al-doped ZnO NPs at various conditions. Fig. 7(a) shows the response of the sample toward 1 ppm of various gases—acetone, NH_3, CO, and isoprene—at 500 °C. The Al-doped ZnO NPs exhibited a very high response for acetone compared with the other gases. Fig. 7(b) shows the sensing response of undoped and doped ZnO NPs with respect to the acetone concentration under the humid condition of 90% RH. In fact, the sensing response of all the samples of the undoped and Al-, Co-, and Cu-

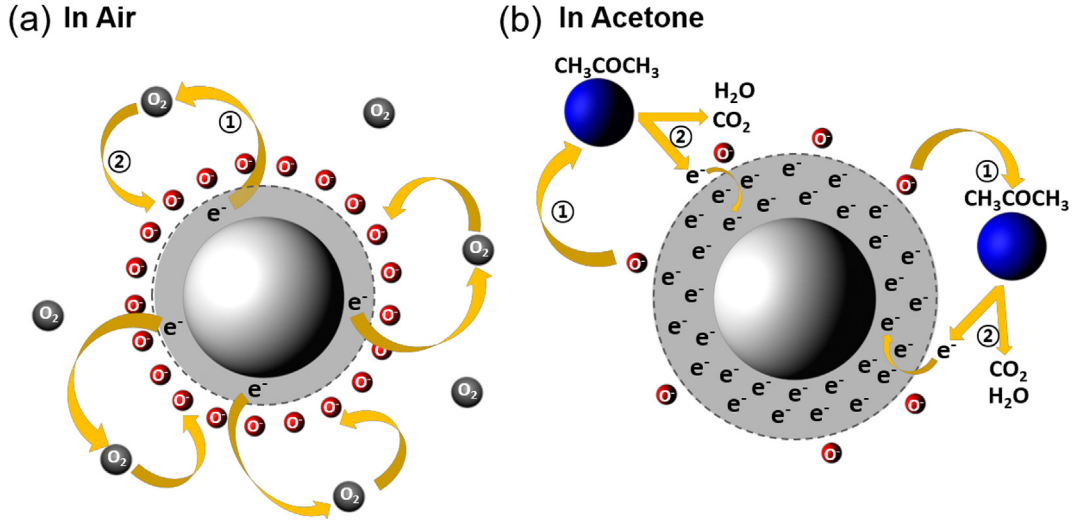

Fig. 6. Schematic of the sensing reaction mechanism of Al-doped ZnO NPs (a) in air and (b) in acetone.

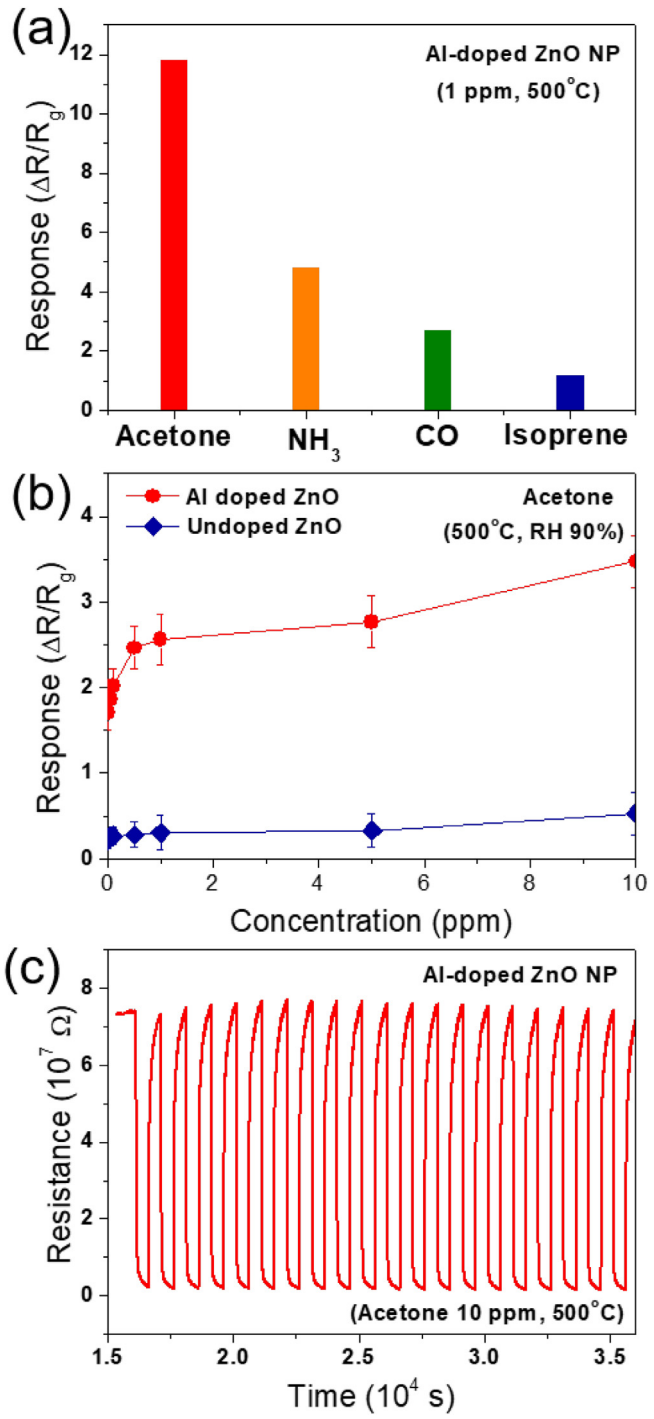

Fig. 7. (a) Responses of Al-doped ZnO NPs for 10 ppm of various target gases, such as acetone, NH_3, and isoprene at 500 °C; (b) sensing responses of the undoped and Al-doped ZnO NPs with respect to the acetone concentration under 90% RH at 500 °C; (c) reproducibility of Al-doped ZnO NPs for the detection of 10-ppm acetone for 20 cycles at 500 °C.

doped ZnO NPs decreased significantly at the high humidity of 90% RH compared to the non-humid condition (Fig. 4(a)). The reduced responses of the samples at 90% RH showed the same tendency depending on the doping elements, as that observed under the dry condition (Fig. 4(a)). The decrease of the sensing response is because of the contamination of the reactive sites of the samples by the adsorption of water molecules. The Al-doped ZnO NPs showed the best response even under humid conditions. The sensing responses of the Al-doped ZnO NPs at 90% RH were ~1.7 at 0.01 ppm and ~3.5 at 10 ppm. Nonetheless, the results indicate that the Al-doped ZnO NPs can detect low concentrations of acetone in exhaled breath. The reproducibility of the sensing performance of the Al-doped ZnO NPs was tested at a fixed gas concentration of 10 ppm during 20 gas in/out cycles. The response/recovery behavior of the Al-doped ZnO NPs indicated that the resistance recovered to its full value after 20 cycles, as shown in Fig. 7(c).

Recently, to obtain the acetone selectivity of a ZnO-based sensor versus other interfering gases in exhaled breath, we performed a study on the detection of acetone in exhaled breath using a miniaturized GC containing Al-doped ZnO QDs (average size of ~5 nm) [34]. We found that acetone was separated through the GC, and a low concentration (0.1 ppm) of acetone was detected effectively owing to the quantum size effect of the Al-doped ZnO QDs [34]. Here, we tested the selective detection of acetone using the miniaturized GC integrated with the Al-doped ZnO NPs (average size of ~20 nm), which were larger than the QDs. Fig. 8(a) shows the miniaturized GC device, which had dimensions of $8 \times 13 \times 16\ cm^3$. Fig. 8(b) presents a schematic of the interior of the device, which comprised a sampling loop, a packed column, three solenoid valves, a miniature pump, and a sensor based on Al-doped ZnO NPs. A schematic of the gas-separation mechanism of the gas mixture through the packed column is presented in Fig. 8(c). The mixed gases are separated with a time difference owing to the different strengths of interaction between the stationary phase of the packed column and the gas molecules. The interaction strength depends on the polarity and weight of the gas molecules because the filler material has a weak polarity. Thus, non-polar and light molecular gases (e.g. N_2 and CO_2) are rapidly released than polar and heavy molecular gases (e.g. acetone). The separated target gas through the column was detected on the Al-doped ZnO NP sensor after a few minutes from injection. The detailed sensing process of the manufactured mini-GC is described in previous studies [34,35].

Fig. 9 shows the change of the sensor signal with time when dry air and acetone of various concentrations (0.5–50 ppm) in air were injected into the miniaturized GC equipped with the Al-doped ZnO NPs at 430 °C. The temperature of 430 °C was found to be the optimal operating temperature for Al-doped ZnO NPs, resulting in the highest sensing responses. Only the acetone chromatogram exhibits a noticeably large peak at ~25 s. The inset of Fig. 9 shows the peak heights (Δ Sensor signal) of the sensor signal, which were obtained from the curves in Fig. 9, with respect to the acetone concentration. The peak height, which indicates the sensing performance of the device, increases with the acetone concentration. Therefore, the results indicate that 0.5 ppm acetone can be selectively detected in air within ~25 s using the miniaturized GC integrated with the Al-doped ZnO NP sensor. Thus, a low concentration of acetone can be sensitively and selectively detected using Al-doped ZnO NPs (~20 nm) significantly larger than QDs (~5 nm).

4. Conclusions

We investigated the effects of the dopants Al, Cu, and Co on the gas-sensing properties of ZnO NPs for the detection of acetone under dry and humid conditions. All the sensor materials were synthesized via hydrothermal methods. The substitution of dopants into the ZnO NPs produced a polycrystalline wurtzite-structured phase with a distribution of particles 15–30 nm in size. Among the various samples, the Al-doped ZnO NPs showed the highest response of 11.8 when exposed to 1 ppm acetone at the optimum operating temperature of 500 °C. The Al-doped ZnO NPs exhibited a response of ~1.7 to the low acetone concentration of 0.01 ppm at 90% RH. Furthermore, we demonstrated that the Al-

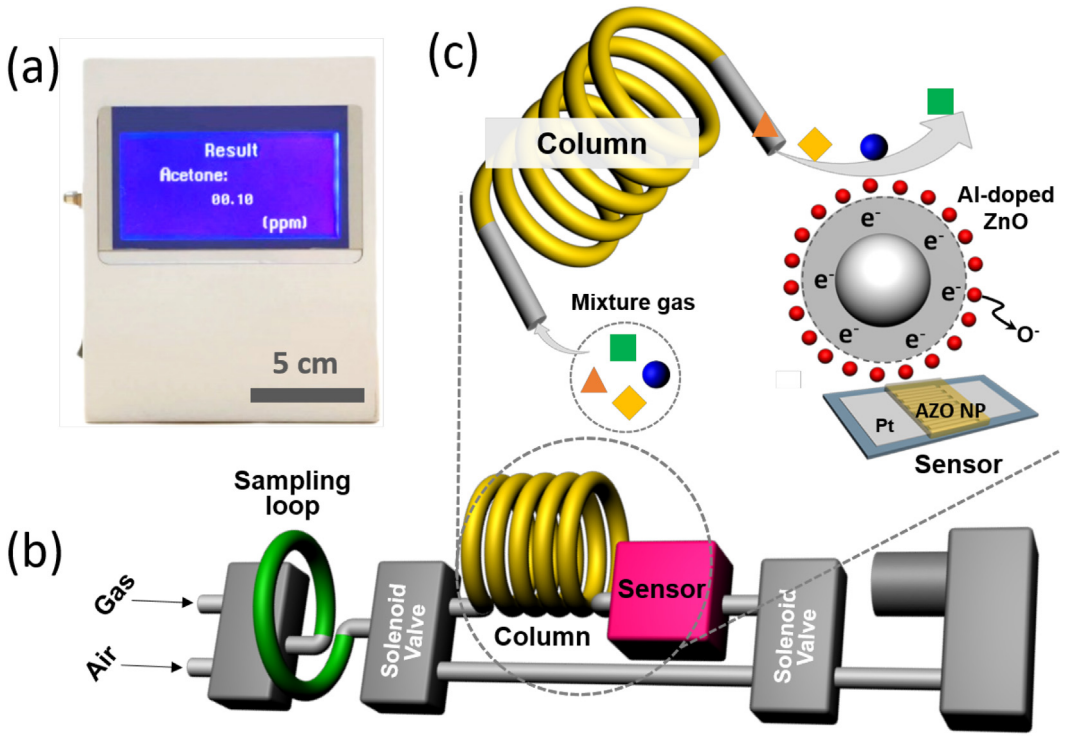

Fig. 8. (a) Miniaturized GC device; (b) schematic showing the interior components of the device; (c) schematic showing the separation mechanism of the gas mixture through the packed column.

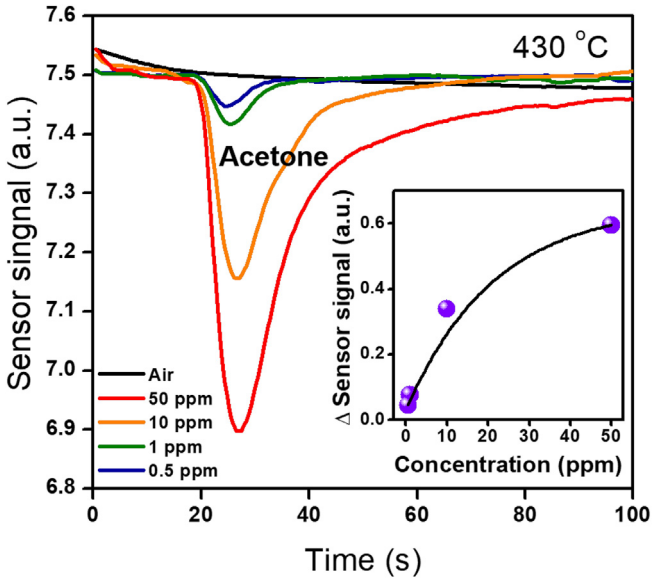

Fig. 9. Sensor signal (log(R)) changes for various acetone concentrations (0.5–50 ppm) and air. The inset shows the peak height of Δ Sensor signal with respect to the acetone concentration.

doped ZnO NPs could sensitively and selectively detect acetone in an air environment by utilizing a miniaturized GC. Yellow emissions in the PL spectrum indicated that a large number of doubly charged oxygen vacancies functioning as donors facilitated the adsorption of oxygen on the surface and the rapid surface reactions for acetone in the Al-doped ZnO NPs, yielding improved sensing performance suitable for application in acetone breath analyzers.

Acknowledgements

This research was supported by the Basic Science Research Program through the National Research Foundation of Korea (NRF) (2017M3A9F1052297), the Medium and Large Complex Technology Commercialization Project through the Commercialization Promotion Agency for R&D Outcomes (2019K000045), and the Priority Research Centers Program through the NRF (2019R1A6A1A11055660).

References

[1] D. Guo, D. Zhang, N. Li, L. Zhang, J. Yang, IEEE Trans. Biomed. Eng. 57 (2010) 2753–2763.
[2] C. Ortiz-Lopez, R. Lomonaco, B. Orsak, J. Finch, Z. Chang, V.G. Kochunov, J. Hardies, K. Cusi, Diabetes Care 35 (2012) 873–878.
[3] T.C. Minh, D. Ray Blake, P.R. Galassetti, Diabetes Res. Clin. Pract. 97 (2012) 195–205.
[4] J.C. Anderson, W.J.E. Lamm, M.P. Hlastala, J. Appl. Physiol. 100 (2006) 880–889.
[5] P. Spanel, K. Dryahina, A. Rejskova, T.W.E. Chippendale, D. Smithm, Physiol. Meas. 32 (2011) N23–N31.
[6] J.C. Anderson, Obesity 23 (2015) 2327–2334.
[7] W. Miekisch, J.K. Schubert, D.A. Vagts, K. Geiger, Clin. Chem. 47 (2001) 1053–1060.
[8] N. Makisimovich, V. Vorotyntsev, L.N. Nikitin, O. Kaskevich, P. Karabun, F. Martynenko, Sens. Actuators, B 36 (1996) 419–421.
[9] A. Kachanov, A. Charvat, F. Stoeckel, J. Opt. Soc. Am. B 12 (1995) 970–979.
[10] M. Righettoni, A. Tricoli, J. Breath Res. 5 (2011), 037109.
[11] P. Song, Q. Wang, Z. Yang, Sensor. Actuator. B Chem. 173 (2012) 839–846.
[12] S. Singkammo, A. Wisitsoraat, C. Sriprachuabwong, A. Tuantranont, S. Phanichphant, C. Liewhiran, ACS Appl. Mater. Interfaces 7 (2015) 3077–3092.
[13] Z. Zhang, Z. Wen, Z. Yea, L. Zhu, RSC Adv. 5 (2015), 59976-56285.
[14] X.L. Xu, Y. Chen, S.Y. Ma, W.Q. Lia, Y.Z. Mao, Sensor. Actuator. B Chem. 213 (2015) 222–233.
[15] M.H. Darvishnejad, A.A. Firooz, J. Beheshtian, A.A. Khodadadi, RSC Adv. 6 (2016) 7838–7845.
[16] X. Zhou, B. Wang, H. Sun, C. Wang, P. Sun, X. Li, X. Hu, G. Lu, Nanoscale 8 (2016) 5446–5453.
[17] X. Li, C. Wang, H. Guo, P. Sun, F. Liu, X. Liang, G. Lu, ACS Appl. Mater. Interfaces

7 (2015) 17811–17818.
[18] M.R. Alenezi, S.J. Henley, N.G. Emersona, S.R.P. Silva, Nanoscale 6 (2014) 235–247.
[19] M. McCune, W. Zhang, Y. Deng, Nano Lett. 12 (2012) 3656–3662.
[20] P. Ilanchezhiyan, G. Mohan Kumar, Xiao Fu, A. Madhankumar, C. Siva, S.U. Yuldashev, H.D. Cho, T.W. Kang, Interfacial charge transfer in ZnTe/ZnO nano arrayed heterostructures and their improved photoelectronic properties, Sol. Energy Mater. Sol. Cells 183 (2018) 73–81.
[21] J. Luo, Y.X. Wang, J. Sun, Z.S. Yang, Q.F. Zhang, MnS passivation layer for highly efficient ZnO–based quantum dot-sensitized solar cells, Sol. Energy Mater. Sol. Cells 187 (2018) 199–206.
[22] H. Zheng, Z.X. Mei, Z.Q. Zeng, Y.Z. Liu, L.W. Guo, J.F. Jia, Q.K. Xue, Z. Zhang, X.L. Du, Fabrication and characterization of high quality n-ZnO/p-GaN heterojunction light emission diodes, Thin Solid Films 520 (2011) 445.
[23] H. Zheng, M. Gruyters, E. Pehlke, R. Berndt, "Magic" vicinal zinc oxide surfaces, Phys. Rev. Lett. 111 (2013), 086101.
[24] W. Zheng, R. Lin, D. Zhang, L. Jia, X. Ji, F. Huang, Adv. Optical Mater. 6 (2018) 1800697.
[25] Z. Zang, Appl. Phys. Lett. 112 (2018), 042106.
[26] C. Li, C. Han, Y. Zhang, Z. Zang, M. Wang, X. Tang, J. Du, Sol. Energy Mater. Sol. Cells 172 (2017) 341–346.
[27] Z. Zang, X. Tang, J. Alloy. Comp. 619 (2015) 98–101.
[28] N.L. Hadipour, A. Ahmadi Peyghan, H. Soleymanabadi, J. Phys. Chem. C 119 (2015) 6398–6404.
[29] R. Yoo, D. Li, H.J. Rim, S. Cho, H.-S. Lee, Sensor. Actuator. B Chem. 266 (2018) 883–888.
[30] R. Yoo, S. Cho, M.-J. Song, W. Lee, Sensor. Actuator. B Chem. 221 (2015) 217–223.
[31] R. Yoo, D. Lee, S. Cho, W. Lee, Sensor. Actuator. B Chem. 254 (2018) 1242–1248.
[32] A. Matyott, F. Buckley, Table of Dielectric Constant and Electric Dipole Moments of Substances in the Gaseous State, U.S. Department of Commerce, National Bureau of Standards, 1953.
[33] C. Singh, E. Panda, RSC Adv. 6 (2016) 48910–48918.
[34] H. Jung, W. Cho, R. Yoo, H.-S. Lee, Y.-S. Choe, J.Y. Jeon, W. Lee, Sensor. Actuator. B Chem. 274 (2018) 527–532.
[35] J.H. Lee, H. Jung, R. Yoo, Y. Park, H.-S. Lee, Y.-S. Choe, W. Lee, Sensor. Actuator. B Chem. 284 (2019) 444–450.
[36] Y. Park, R. Yoo, S. Park, J.H. Lee, H. Jung, H. Lee, W. Lee, Sensor. Actuator. B Chem. 290 (2019) 258–266.
[37] S.U. Awan, S.K. Hasanain, G. Hassnain Jaffari, D.H. Anjum, U.S. Qurashi, J. Appl. Phys. 116 (2014), 083510.
[38] E.J. Guielli, O. Baffa, D.R. Clarke, Sci. Rep. 5 (2015) 14004.
[39] C. Singh, E. Panda, RSC Adv. 6 (2016) 48910–48918.
[40] S. Bai, S. Chen, Y. Zhao, T. Guo, R. Luo, D. Li, A. Chen, J. Mater. Chem. 2 (2014) 16697–16706.
[41] S.M. Chou, L.G. Teoh, W.H. Lai, Y.H. Su, M.H. Hon, Sensors 6 (2006) 1420–1427.
[42] N. Singh, C. Yan, P.S. Lee, Sens. Actuators, B 150 (2010) 19–24.
[43] T.H. Risby, S.F. Solga, Appl. Phys. B Laser Opt. 85 (2006) 421–426.
[44] L. Ferrus, H. Guenard, G. Vardon, P. Varene, Respir. Physiol. 39 (1980) 367–381.